Ann Rheum Dis 000 (2025) 1–13

Contents lists available at ScienceDirect

Annals of the Rheumatic Diseases

journal homepage: https://www.sciencedirect.com/journal/annals-of-the-rheumatic-diseases

Systemic lupus erythematosus

Integrative spatial multiomics analysis reveals regulatory mechanisms of VCAM1 $^{+}$ proximal tubule cells in lupus nephritis

Junyu Wang[1,2], Ao Zheng[1,2], Nianping Liu[1,3], Zhen Tan[1], Yu Shi[2], Tianyi Ma[2], Songwen Luo[2], Lin Zhu[2], Zhou Zhou[1], Feifei Yuan[4], Tiekun Li[5], Yuyan Gong[6], Jingwen Fang[2,7], Lu Liu[8], Xuejun Zhang[8], Sang-Cheol Bae[9], Chikashi Terao[10], Zhu Chen[1], Xiaomei Li[1], Guosheng Wang[1,*], Kun Qu[1,2,3,11,*], Chuang Guo[1,2,12,*]

[1] *Department of Rheumatology and Immunology, The First Affiliated Hospital of USTC, State Key Laboratory of Eye Health, Division of Life Sciences and Medicine, School of Basic Medical Sciences, University of Science and Technology of China, Hefei, China*
[2] *Division of Life Sciences and Medicine, University of Science and Technology of China, Hefei, China*
[3] *School of Biomedical Engineering, Suzhou Institute for Advanced Research, University of Science and Technology of China, Suzhou, China*
[4] *Division of Nephrology, Nanfang Hospital, Southern Medical University, Guangzhou, China*
[5] *Nanjing Kingmed Center for Clinical Laboratory Co, Ltd, Nanjing, Jiangsu, China*
[6] *SeekGene BioSciences Co, Ltd, Beijing, China*
[7] *HanGene Biotech, Hefei, Anhui, China*
[8] *Institute of Dermatology, Anhui Medical University, Anhui, China*
[9] *Department of Rheumatology, Hanyang University Hospital for Rheumatic Diseases, Hanyang University Institute for Rheumatology Research, Hanyang Institute of Bioscience and Biotechnology, Seoul, Republic of Korea*
[10] *Laboratory for Statistical and Translational Genetics Analysis, RIKEN Center for Integrative Medical Sciences, Wako, Saitama, Japan*
[11] *Institute of Artificial Intelligence, Hefei Comprehensive National Science Center, Hefei, China*
[12] *School of Pharmacy, Bengbu Medical University, Bengbu, China*

ARTICLE INFO

Article history:
Received 9 February 2025
Received in revised form 20 July 2025
Accepted 14 August 2025

Handling editor Josef S Smolen

ABSTRACT

Objectives: Lupus nephritis (LN) is a severe complication of systemic lupus erythematosus (SLE), characterised by kidney inflammation, tubular injury, and interstitial fibrosis. However, the spatial organisation of these heterogeneous cell populations and their regulatory mechanisms in LN remain poorly understood. The objective of this study was to investigate the regulatory mechanisms underlying region-specific kidney lesions and tubular damage in LN.

Methods: We performed single-cell multiome and spatial transcriptomic analyses on kidney biopsy samples from patients with LN and controls, integrating data from the largest East Asian SLE genome-wide association studies (GWAS) (208,370 samples) to date. Validation experiments were performed using multiplex immunohistochemistry (mIHC), *in vitro* lentiviral-mediated transcription factor overexpression, and functional stimulation assays.

Results: We identified *VCAM1*-expressing proximal tubule (PT_VCAM1) cells as components of an LN-specific inflammatory niche (niche 5) localised in the kidney cortex. Both in silico and *in vitro* experiments demonstrated that interactions between PT_VCAM1 cells and myofibroblasts,

*Correspondence to Dr Chuang Guo, Kun Qu, Guosheng Wang.
E-mail addresses: gswang0551@163.com (G. Wang), qukun@ustc.edu.cn (K. Qu), gchuang@ustc.edu.cn (C. Guo).
Junyu Wang, Ao Zheng, and Nianping Liu contributed equally to this work.

https://doi.org/10.1016/j.ard.2025.08.015

Please cite this article as: J. Wang et al., Integrative spatial multiomics analysis reveals regulatory mechanisms of VCAM1 $^{+}$ proximal tubule cells in lupus nephritis, Ann Rheum Dis (2025), https://doi.org/10.1016/j.ard.2025.08.015

as well as immune cells in niche 5, promote their epithelial-mesenchymal transition. Trajectory analysis suggested that PT_VCAM1 cells originate from a failed-repair pathway in proximal tubule cells, regulated by transcriptional networks involving BACH2. Integrative GWAS analysis further linked SLE-associated risk single-nucleotide polymorphisms to *cis*-regulatory elements specific to PT_VCAM1 cells, including single-nucleotide polymorphisms within the distal enhancer of the *BMP2K* locus, which establishes a BACH2 motif.

Conclusions: Collectively, our findings characterise PT_VCAM1 cells as injury-responsive cell states that contribute to the inflammatory and fibrotic niche in LN, linking genetic predisposition to cellular injury and disease progression.

KEY MESSAGES

WHAT IS ALREADY KNOWN ON THIS TOPIC

- Lupus nephritis (LN) is a severe complication of systemic lupus erythematosus (SLE), characterised by tubular epithelial dysfunction, immune cell infiltration, and progressive fibrosis.
- Recent studies have identified key LN-associated immune cell subpopulations, such as granzyme K^+ CD8 T cells and $CD163^+$ dendritic cells.
- Genome-wide association studies (GWAS) have identified susceptibility candidates that contribute to the dysfunction of immune subpopulations in SLE.

WHAT THIS STUDY ADDS

- Using single-cell multiome and spatial transcriptomic sequencing, we identified a distinct inflammatory microenvironment in the renal cortex of patients with LN (niche 5), characterised by the colocalisation of *VCAM1*-expressing proximal tubule (PT_VCAM1) cells, myofibroblasts, and immune cells.
- PT_VCAM1 cells exhibited a "failed-repair" phenotype, regulated by a core transcriptional network involving 4 transcription factors, with BACH2 emerging as a potential novel therapeutic target.
- The increased presence of myofibroblasts and immune cells within niche 5 facilitated interactions with PT_VCAM1 cells through several ligands, including COL4A1, SPP1, and transforming growth factor (TGF)-β1, thereby promoting epithelial-mesenchymal transition (EMT) in PT_VCAM1 cells.
- Integrative GWAS analysis revealed associations between SLE risk single-nucleotide polymorphisms (SNPs) and PT_VCAM1-specific *cis*-regulatory elements, including variants in the distal enhancer of the *BMP2K* locus. These variants were shown to create a BACH2 motif, reinforcing the failed-repair phenotype in PT_VCAM1 cells.

HOW THIS STUDY MIGHT AFFECT RESEARCH, PRACTICE OR POLICY

- Our study presents a comprehensive mapping of the spatial architecture and regulatory mechanisms in the human LN kidney, revealing spatial and genetic influences on PT_VCAM1 cells in promoting inflammatory and fibrotic remodelling.
- Our multiomics strategy, which identified causal variants specific to distinct cell subpopulations, offers a framework for developing precision therapeutics targeting cell types implicated in LN pathogenesis.

INTRODUCTION

Lupus nephritis (LN) is a severe complication of systemic lupus erythematosus (SLE), affecting up to two-thirds of patients with SLE and contributing to morbidity and mortality [1]. LN is characterised by immune cell infiltration, tubular epithelial injury, and progressive fibrosis. Immune cells, including macrophages, T cells, and B cells, infiltrate kidney tissues and initiate inflammatory responses that exacerbate fibrosis and kidney damage [2,3]. Tubular epithelial cells, particularly proximal tubule (PT) cells, also contribute to local inflammation through the secretion of inflammatory mediators and interactions with immune and stromal cells [4,5]. Elucidating these interactions within their spatial context is fundamental to advancing our understanding of LN pathogenesis.

Recent single-cell sequencing studies have identified transcriptional programs in LN-associated immune cell subpopulations, such as $APOE^+$ monocytes, granzyme K^+ CD8 T cells, and $CD163^+$ dendritic cells [2,4,6,7]. However, the role of tubular epithelial subpopulations, such as PT cells in LN, remains insufficiently explored. PT cells are essential for kidney function and exhibit subpopulation-specific heterogeneity in healthy and diseased conditions [5]. For instance, healthy kidneys feature PT-S1, PT-S2, and PT-S3 as primary subpopulations, whereas diseased kidneys exhibit PT cell subpopulations such as *VCAM1*-expressing PT (PT_VCAM1) cells [8,9]. PT_VCAM1 cells are enriched in fibrotic microenvironments and are implicated in immune cell recruitment and inflammation [10]. Despite these insights, the mechanisms driving the transition of conventional PT cells into PT_VCAM1 cells and the regulatory pathways associated with this process remain unresolved. Addressing these gaps could provide a mechanistic framework for understanding the progression of LN and other kidney pathologies.

Genetic predispositions significantly contribute to the development of LN, with genome-wide association studies (GWAS) identifying numerous genetic risk variants associated with lupus, primarily in noncoding regions of the genome [11]. These studies implicate *cis*-regulatory elements (CREs) in the regulation of genes associated with LN pathogenesis [12,13]. However, challenges remain in prioritising these variants to specific cellular populations as well as clarifying how these variants affect cellular function or contribute to disease pathogenesis. Integrating GWAS data with single-cell and spatial transcriptomics (STs) offers a systematic framework to link CREs with specific cell types and evaluate their influence on transcriptional regulation in LN.

This study integrates single-cell multiome sequencing and ST to delineate cellular niches, intercellular interactions, and genetic regulatory mechanisms in LN kidneys. We identified 6 kidney niches, including an inflammatory niche (niche 5) in the kidney cortex of patients with LN, which is enriched with immune cells, myofibroblasts (MyoFIB), and PT_VCAM1 cells. PT_VCAM1 cells exhibited a profibrotic and proinflammatory phenotype, arising from a failed-repair pathway regulated by BACH2. Integrative GWAS fine-mapping linked SLE-associated single-nucleotide polymorphisms (SNPs) to PT_VCAM1-specific CREs. These findings highlight spatial and genetic influences on PT_VCAM1 cells in promoting inflammatory and fibrotic remodelling in LN kidneys.

METHODS

Details of the methods are available in the online Supplementary Methods.

RESULTS

Multimodal single-cell profiling of kidney cells in human LN

We obtained kidney tissue samples from 8 patients with LN and used adjacent nontumour tissues from 2 patients with kidney tumour as control samples (Supplementary Table S1). We then performed paired single-nucleus RNA sequencing (snRNA-seq) and single-nucleus assay for transposase-accessible chromatin sequencing (snATAC-seq) using the 10× multiome platform, which enables the concurrent measurement of RNA expression and chromatin accessibility within the same nuclei (Fig 1A and Supplementary Fig S1A). After rigorous filtering of RNA and chromatin accessibility data, we retained 41,543 high-quality nuclei. To expand our dataset, we integrated additional snRNA-seq and snATAC-seq datasets from 5 control samples [8]. Unlike our paired dataset, these public datasets contain separate populations of nuclei for snRNA-seq and snATAC-seq from the same samples. In total, this integration resulted in 64,479 nuclei for snRNA data and 72,472 nuclei for snATAC data, with each nucleus containing an average of 2078 genes and 17,523 fragments (Supplementary Fig S1B).

Following batch effect correction across samples and unsupervised clustering, we identified 35 distinct cell subpopulations in the transcriptomic data, subsequently categorised into 13 cell types (Fig 1B-D and Supplementary Fig S1C-E). These cell subpopulations represented a wide range of kidney cell types, including those located in the cortex, medullary ray, and outer medulla. Moreover, the identified cell subpopulations exhibited extensive similarities to those derived from publicly available human kidney cell datasets [3,8] (Supplementary Fig S1F,G), validating the accuracy of the cell clustering. Additionally, leveraging the high-resolution cell subpopulation annotations obtained from snRNA-seq, we used the Seurat label transfer approach [14] to map these annotations to the snATAC-seq cells. This process resulted in cell cluster annotations within the snATAC-seq data that showed high consistency with those identified in publicly available snATAC-seq data from human kidney cells [3] (Fig 1C and Supplementary Fig S2A,B).

To evaluate cellular and molecular alterations between LN samples and control samples, we quantified the proportions of each identified cell type relative to the total cell population, as well as the number of differentially expressed genes (DEGs) and differentially accessible regions (DARs) by comparing LN samples with control samples within each cell type (Fig 1E,F and Supplementary Table S2). In patients with LN, we observed a significant increase in the proportion of infiltrating immune cells (Padjusted = .014), consistent with previous reports, indicating that enhanced immune activation contributes to LN pathogenesis [4]. Furthermore, we found a significant reduction in podocyte populations (Padjusted = .0041), in line with histopathological evidence that podocyte loss compromises glomerular filtration integrity [15]. Although the proportion of PT cells did not show a statistically significant change, this cell type exhibited the highest number of DEGs and DARs, indicating extensive alterations in their biological function in LN. Collectively, our multiome atlas provided a detailed molecular characterisation of LN, revealing substantial changes in both cell-type proportions and gene expression profiles compared with controls.

Niche 5 is characterised by increased MyoFIB, immune infiltrates, and PT_VCAM1 cells

To investigate the cellular neighbourhoods surrounding significantly altered cell subpopulations, we prepared 10-μm cryosections from 11 kidney tissue samples for ST profiling, comprising 8 from patients with LN and 3 from control samples (Fig 2A and Supplementary Fig S1). We also expanded our cohort by incorporating 1 publicly available control sample from the study by Melo Ferreira et al [16]. After stringent quality control, our ST dataset comprised 6410 spots, with an average of 17 cells and 3292 detected genes per spot (Supplementary Fig S3A,B). We then applied Cell2location [17] to assign cell-type probabilities to each spot and subsequently used SPACEL [18] for joint analysis across all slices, identifying 6 distinct cellular niches (niche 1-6) in patients with LN and control samples (Fig 2B and Supplementary Fig S3C,D). Pathologist annotations of haematoxylin and eosin (H&E)-stained images delineated the cortical, medullary ray, and outer medulla regions (Fig 2C and Supplementary Fig S3E).

Notably, niche 5 was significantly enriched in the cortical region of LN samples, whereas niche 2 predominated in the cortex of control samples (Fig 2D and Supplementary Fig S3F,G). These 2 niches recapitulated known tissue features, representing kidney tubules (niche 2) and atrophied kidney tubules (niche 5), respectively (Supplementary Fig S4A). Other niches, including niche 1 (cortex), niche 3 (medullary rays), and niche 4 (outer medulla), showed no significant differences between LN and control samples (Supplementary Fig S3F,G). Further analysis of the cell type composition of LN/control-enriched niches revealed that niche 5 was notably enriched with MyoFIB, PT_VCAM1 cells, and various immune cell populations, including *CD163*-expressing M2 macrophages (Mac_M2), *ITGAX*-expressing macrophages (Mac_ITGAX), CD8 T cells, and plasma cells (Fig 2E-H and Supplementary Fig S4B). Cell types within niche 5 exhibited higher colocalisation scores compared with those in other niches, suggesting a distinct microenvironment structure (Supplementary Fig S4C). Moreover, Moran's I analysis revealed that PT_VCAM1 cells exhibited significantly increased spatial aggregation in LN kidneys (Supplementary Fig S4D).

To validate the presence of a cellular neighbourhood coenriched with MyoFIB, PT_VCAM1 cells, and immune cells in the cortex of patients with LN, we first utilised SeekSpace to analyse the spatial coordinates of bona fide single-cell transcriptomes from an additional patients with LN across 2 replicates. This approach identified high-quality single cells and successfully mapped 27 out of 35 cell subpopulations in 10× multiome datasets (Supplementary Fig S5A-E). We observed spatial colocalisation of PT_VCAM1 cells, MyoFIB, and immune cells in the cortical regions (Supplementary Fig S5F,G). Furthermore, we performed multiplex immunohistochemistry (mIHC) staining using 4′,6′-dia midino-2-phenylindole (DAPI) and antibodies targeting AQP1, VCAM1, α-SMA (*ACTA2*), and CD45 (*PTPRC*) in 3 LN samples and 3 control samples. The results revealed significantly higher numbers of PT_VCAM1 cells, MyoFIB, and immune cells in the cortical region of patients with LN (Fig 2I, J), with these cell types showing close spatial proximity to each other (Supplementary Fig S6A).

DEG analysis across distinct cellular niches revealed that niche 5 exhibited elevated expression of complement genes

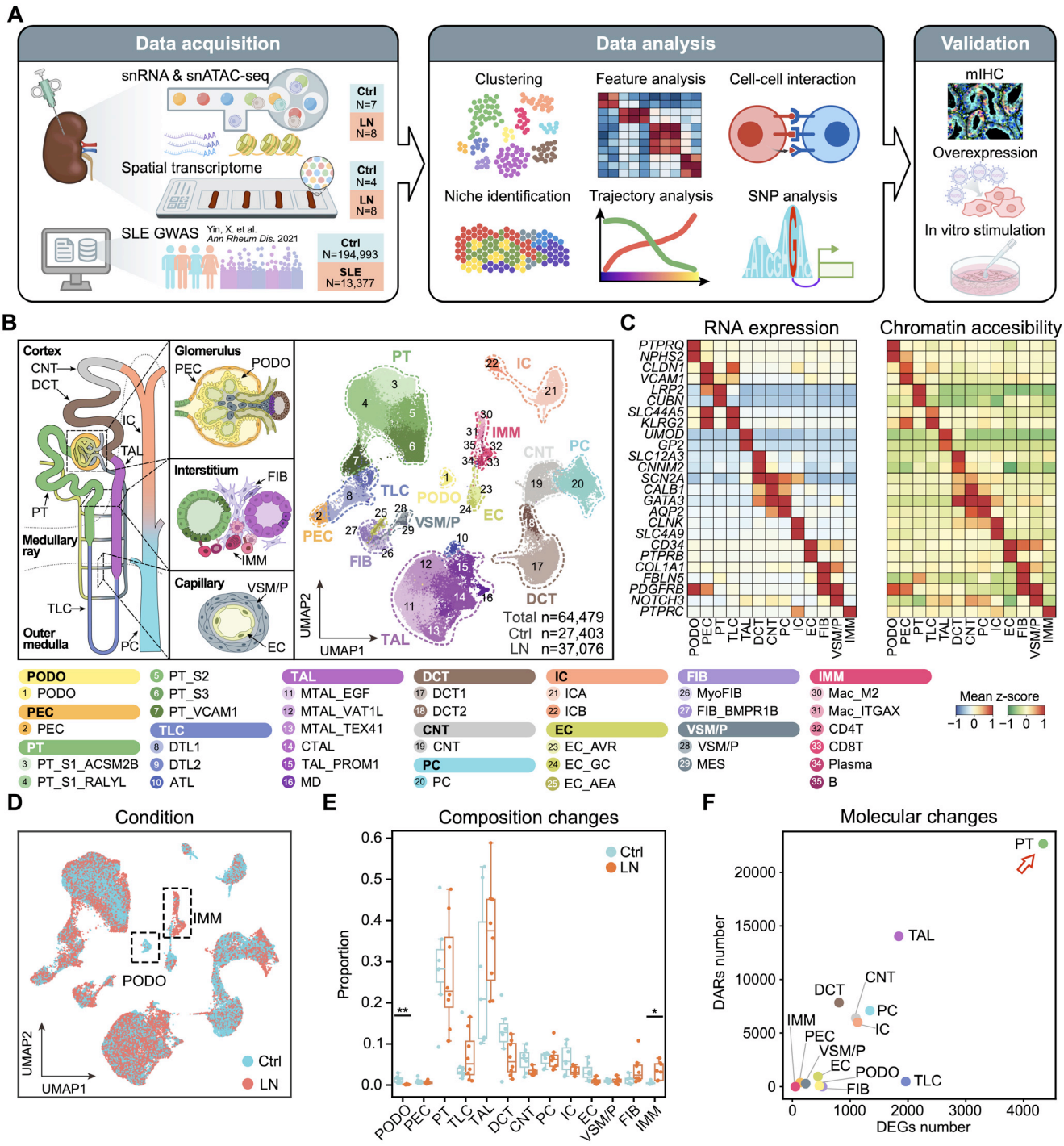

Figure 1. Single-cell multiomics profiling of human lupus nephritis (LN). A, Schematic overview of the study design. B, Scheme of the kidney, with cell-type distribution indicated by colour (left), and uniform manifold approximation and projection (UMAP) visualisation of single-nucleus RNA sequencing (snRNA-seq) data from all samples, coloured by cell subpopulations (right). Dashed circles highlight cell types. C, Heatmaps showing z-score−transformed gene expression (left) and chromatin accessibility (right) of canonical marker genes across the 13 cell types. D, UMAP visualisation of snRNA-seq data from all samples, coloured by condition. Cell types with significant proportional differences between control (Ctrl) and LN are highlighted with dashed rectangles. E, Box plots comparing the cell proportion of each cell type between Ctrl and LN samples. Statistical significance was assessed using a 2-sided Wilcoxon rank-sum test, and *P* values were adjusted using the Benjamini-Hochberg correction (*Padjusted < .05; **Padjusted < .01). F, Scatter plot showing the number of differentially expressed genes (DEGs) and differentially accessible regions (DARs) across the 13 cell types, comparing LN and Ctrl conditions. snATAC-seq, single-nucleus assay for transposase-accessible chromatin sequencing; SLE, systemic lupus erythematosus; SNP, single-nucleotide polymorphism; mIHC, multiplex immunohistochemistry; PODO, podocyte; PEC, parietal epithelial cell; PT, proximal tubule cell; TLC, thin limb cell; TAL, thick ascending limb cell; DCT, distal convoluted tubule cell; CNT, connecting tubule cell; PC, principal cell; IC, intercalated cell; EC, endothelial cell; FIB, fibroblast; VSM/P, vascular smooth muscle cell or pericyte; IMM, immune cell; PT_VCAM1, *VCAM1*-expressing proximal tubule cell; DTL1, descending thin limb cell type 1; DTL2, descending thin limb cell type 2; ATL, ascending thin limb cell; MTAL_EGF, *EGF-expressing* medullary thick ascending limb cell; MTAL_VAT1L, *VAT1L-expressing* medullary thick ascending limb cell; MTAL_TEX41, *TEX41-expressing* medullary thick ascending limb cell; CTAL, cortical thick ascending limb cell; TAL_PROM1, *PROM1-expressing* thick ascending limb cell; MD, macula densa cell; DCT1, distal convoluted tubule cell type 1; DCT2, distal convoluted tubule cell type 2; ICA, alpha-intercalated cell; ICB, beta-intercalated cell; EC_AVR, ascending vasa recta endothelial cell; EC_GC, glomerular capillary endothelial cell; EC_AEA, afferent/efferent arteriole endothelial cell; MyoFIB, myofibroblast; FIB_BMPR1B, *BMPR1B-expressing* fibroblast; MES, mesangial cell; Mac_M2, *CD163-expressing* M2 macrophage; Mac_ITGAX, *ITGAX-expressing* macrophage.

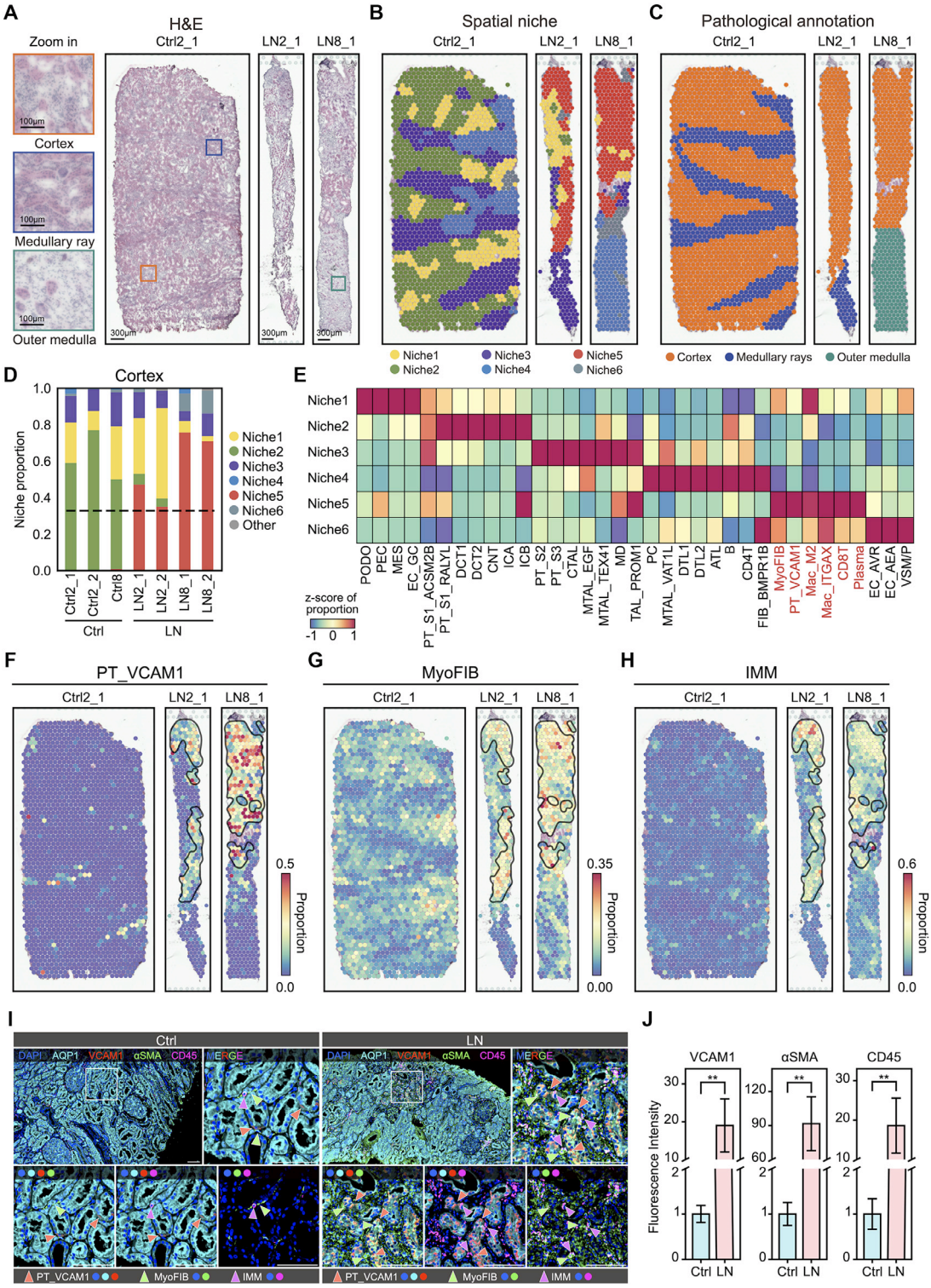

Figure 2. Identification and cellular composition of distinct niches in lupus nephritis (LN). A, Haematoxylin and eosin (H&E)-stained images of representative control (Ctrl) and LN samples, with zoomed-in views of the cortex, medullary rays, and outer medulla regions shown on the left. B and C, Spatial niches (B) and pathological annotations (C) of representative samples. D, Stacked bar plot showing the niche composition in the cortex region. The dashed line indicates the mean proportion of the dominant niche in the cortex region. E, Heatmap showing the cellular composition of cell subpopulations across 6 distinct niches. F-H, Spatial distribution of cellular composition calculated by Cell2location for VCAM1-expressing proximal tubule (PT_VCAM1) cells (F), myofibroblasts (MyoFIB) (G), and immune cells (H) in representative Ctrl and LN samples. Niche 5 is outlined in black lines. I, Multiplex immunohistochemistry (mIHC) staining of representative Ctrl and LN samples, with each panel consisting of 5 subpanels: 1 full image and 4 magnified views of regions outlined by white squares. The zoomed-in views include a merged image and 3 images showing the colocalisation of 2 cell types in pairs. Scale bar = 100 μm. J, Bar plot showing the fluorescence intensity of VCAM1, α-SMA, and CD45 between Ctrl and LN samples. Statistical significance was assessed using a one-sided Student's t-test (**$P < .01$; n = 3 per group). PODO, podocyte; PEC, parietal epithelial cell; PT, proximal tubule cell; DTL1, descending thin limb cell type 1; DTL2, descending thin limb cell type 2; ATL, ascending thin limb cell; MTAL_EGF, *EGF*-expressing medullary thick ascending limb cell; MTAL_VAT1L, *VAT1L*-expressing medullary thick ascending limb cell; MTAL_TEX41, *TEX41*-expressing medullary thick ascending limb cell; CTAL, cortical thick ascending limb cell; TAL_PROM1, *PROM1*-expressing thick ascending limb cell; MD, macula densa cell; DCT1, distal convoluted tubule cell type 1; DCT2, distal convoluted tubule cell type 2; CNT, connecting tubule cell; PC, principal cell; ICA, alpha-intercalated cell; ICB, beta-intercalated cell; EC_AVR, ascending vasa recta endothelial cell; EC_GC, glomerular capillary endothelial cell; EC_AEA, afferent/efferent arteriole endothelial cell; FIB_BMPR1B, *BMPR1B*-expressing fibroblast; VSM/P, vascular smooth muscle cell or pericyte; MES, mesangial cell; IMM, immune cell; Mac_M2, *CD163*-expressing M2 macrophage; Mac_ITGAX, *ITGAX*-expressing macrophage.

(eg, *C3* and *C1S*), chemokines (eg, *CCL5* and *CCL19*), and collagen-related genes (eg, *COL3A1* and *COL4A1*), suggesting inflammatory signalling and active extracellular matrix (ECM) remodelling in this niche (Supplementary Fig S7A-C and Supplementary Table S3). To further evaluate the clinical relevance of niche 5, we analysed microarray-derived gene expression profiles of 45 pretreatment patients with LN [19] and assessed correlations with established clinical indicators of disease severity, including serum creatinine and proteinuria levels. The niche 5 signature (ie, DEGs identified in niche 5) showed a positive correlation with both serum creatinine (R = 0.318, P = .033) and proteinuria levels (R = 0.290, P = .053) (Supplementary Fig S7D,E). Collectively, these observations underscore that in the cortical regions of patients with LN, the disruption of normal tissue architecture sustains an inflammatory milieu involving PT_VCAM1 cells, MyoFIB, and immune cells, which is positively correlated with increased disease severity.

PT_VCAM1 cells display a failed-repair state derived from PT_S1_RALYL cells, with their transition regulated by BACH2

PT cells are primary sites of kidney injury and contribute to disease progression across both acute and chronic etiologies [5,20,21]. Given that PT_VCAM1 cells constitute a cellular component of the LN-enriched inflammatory niche (ie, niche 5), we sought to investigate the functional characteristics of PT cells. We identified 5 distinct PT cell subsets (Fig 3A and Supplementary Fig S8A-D), which correspond to the anatomical segments of PT, ranging from PT-S1 (subdivided into PT_S1_ACSM2B and PT_S1_RALYL) to PT-S3. Notably, PT_VCAM1 cells were distinguished by a high expression of injury-associated markers, such as *CDH6, VCAM1*, and *HAVCR1* [3,21,22] (Fig 3B), resembling the *VCAM1*-expressing injured PT cell population previously described as failed-repair PT cells in an ischaemia-reperfusion injury (IRI) mouse model [20]. A hypergeometric test confirmed significant overlap in DEG comparison between PT_VCAM1 cells and failed-repair PT cells (Fig 3C, Supplementary Fig S8E, and Supplementary Table S4).

Notably, similar PT_VCAM1 populations have also been reported in chronic settings such as autosomal dominant polycystic kidney disease (ADPKD), where they contribute to inflammatory and fibrotic responses [9]. Cross-disease comparison (see Supplementary Methods)—including COVID-19-associated acute kidney injury (COV-AKI), acute kidney injury (AKI), diabetic kidney disease (DKD), and hypertensive chronic kidney disease (H-CKD)—revealed that PT_VCAM1 cells in LN exhibited a distinct transcriptomic profile characterised by enhanced activation of interferon-stimulated genes (eg, *IFI44, MX1*, and *IFIT3*) (Supplementary Fig S9A-E), suggesting that the interferon-driven signature of PT_VCAM1 cells is a unique feature of the autoimmune context of LN. Furthermore, deconvolution analysis of bulk transcriptomic data from kidney tissues of 16 patients with proliferative LN—before and after cyclophosphamide treatment [23]—demonstrated that patients with a higher proportion of PT_VCAM1 cells exhibited poorer therapeutic response (P = .0128) (Supplementary Fig S9F). This observation was further supported by analysis of a 45-patient microarray dataset [19], where *VCAM1* expression levels showed a positive correlation with serum creatinine (R = 0.358, P = .016) and proteinuria (R = 0.357, P = .016), highlighting its potential as a biomarker for disease severity and treatment outcome prediction in LN (Supplementary Fig S9G,H).

To investigate whether PT_VCAM1 cells originate from specific PT cell subsets, we applied a diffusion map [24] and PAGA graph [25] to explore potential differentiation trajectories. Both analyses revealed a close relationship between PT_VCAM1 cells and PT_S1_RALYL cells, suggesting a possible lineage connection between the 2 cell clusters (Fig 3D and Supplementary Fig S10A). This hypothesis was further supported by the spatial colocalisation of PT_VCAM1 and PT_S1_RALYL cell clusters within kidney tissue sections (Fig 3E and Supplementary Figs S5G, 10B). A comparative analysis between PT_S1_RALYL and PT_S1_ACSM2B cells, the latter expressing mature PT markers (eg, *ACSM2A* and *SLC22A6*) indicative of a healthy state, revealed that PT_S1_RALYL cells had elevated expression of injury-associated genes (eg, *CDH6, NFIA*, and *NFIB*) (Supplementary Fig S10C,D). This suggested that PT_S1_RALYL cells represent an intermediate injury-responsive state, potentially linking normal PT cells to the injury-prone PT_VCAM1 cells.

Building on this, we utilised both Multivelo [26] and Palantir [27] to infer the differentiation trajectory between PT-S1 cells and PT_VCAM1 cells. Both methods yielded consistent results, delineating 2 distinct differentiation trajectories (Fig 3F). The first trajectory (path 1) connected PT_S1_RALYL cells to PT_S1_ACSM2B cells, suggesting a successful injury-repair pathway. In contrast, the second trajectory (path 2) led from PT_S1_RALYL cells to PT_VCAM1 cells, representing a failed-repair path that results in the injury-associated phenotype. Pseudotime ordering analysis further confirmed these trajectories, showing that path 1 is characterised by a high expression of mature PT markers, such as *ACSM2A* and *ACSM2B,* at its terminal stage (Supplementary Fig S10E-G and Supplementary Table S5). In contrast, path 2 exhibited upregulation in the expression of genes related to proinflammatory responses (eg, *TNFSF10* and *CX3CL1*), profibrotic signalling (eg, *ITGA3* and *COL4A1*), and injury markers (eg, *VIM* and *HAVCR1*) (Fig 3G and Supplementary Fig S10F, G). Consistently, the enhancer landscape along this trajectory revealed progressively increased chromatin accessibility at regulatory regions of the proinflammatory (eg, *CSF1* and *IL32*) and profibrotic genes (eg, *ITGA3* and *COL4A1*) (Supplementary Fig S10H,I). To further explore the regulatory networks underlying these differentiation trajectories, we used SCENIC+ [28] to identify potential transcription factors (TFs). We found that the PT_S1_RALYL cells enriched putative TFs similar to both PT_S1_ACSM2B and PT_VCAM1 cells, indicating that PT_S1_RALYL cells occupy an intermediate state with the potential to differentiate towards either a successful or failed-repair pathway (Fig 3H).

In addition, we examined how TFs specifically regulate the differentiation processes along each trajectory and constructed regulatory networks for both paths (Supplementary Table S6). Peroxisome proliferator-activated receptor alpha (PPARA), a known TF that could protect the kidney against injury [29], was putatively involved in regulating the path 1 process (Supplementary Fig S11A). We also identified 4 core TFs—BACH2, NFAT5, KLF6, and FOSL2—that regulate path2, each targeting more than 50 downstream genes (Fig 3I and Supplementary Fig S11B). NFAT5, a well-established regulator of cellular responses to hypertonic stress, exhibited a positive correlation with the severity of proteinuria in patients with LN [30,31]. Similarly, KLF6, whose loss in PT cells has been shown to protect against kidney fibrosis in mouse models [32], also plays a known regulatory role.

Additionally, we observed that BACH2, a TF associated with oxidative stress and immune response regulation [33], regulates the largest number of downstream genes during the PT_VCAM1

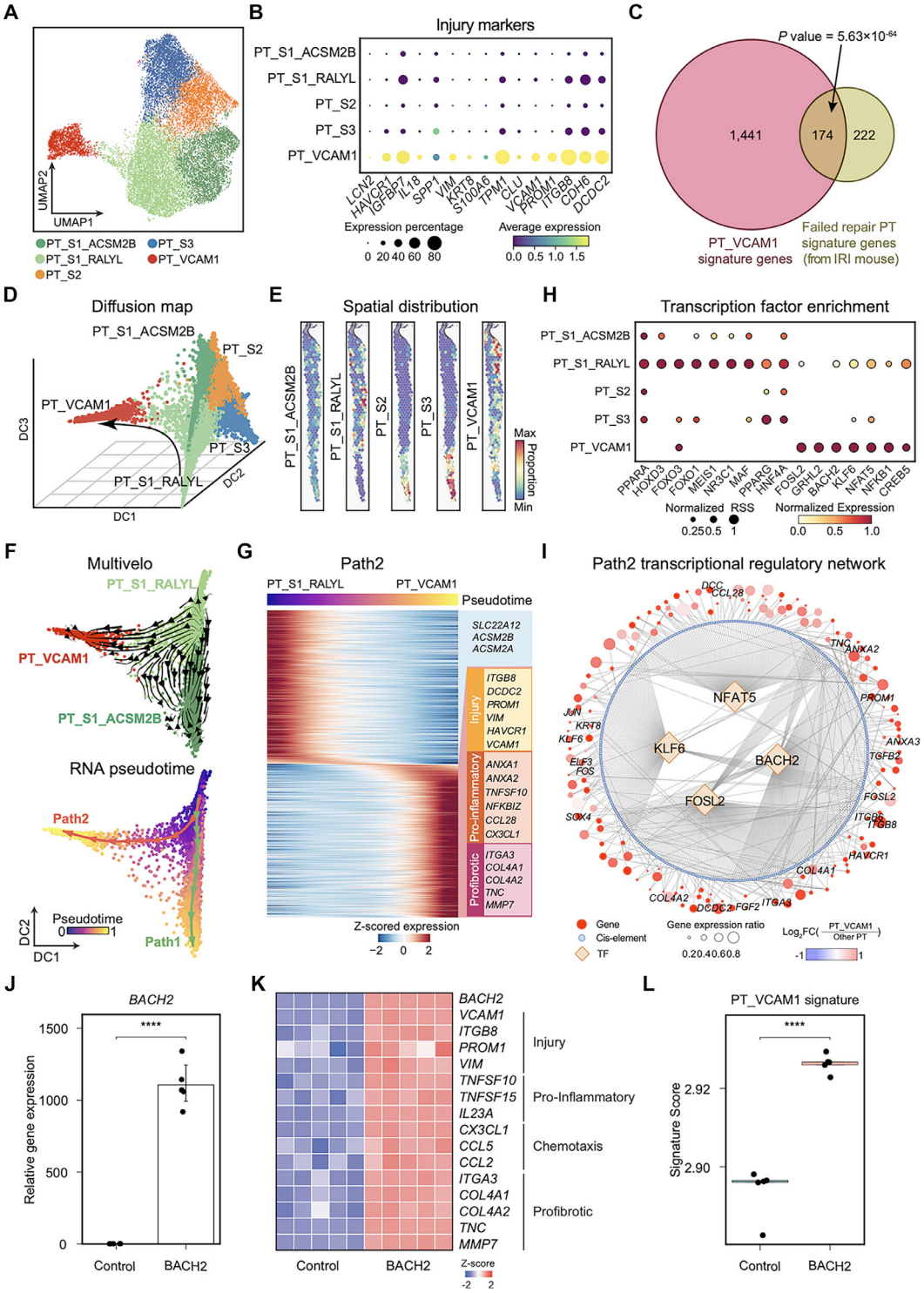

Figure 3. Regulatory networks of *VCAM1*-expressing proximal tubule (PT_VCAM1) cells. A, Uniform manifold approximation and projection (UMAP) visualisation of proximal tubule (PT) cells in single-nucleus RNA sequencing (snRNA-seq data), coloured by PT subpopulations. B, Dot plot showing the average gene expression of injury markers across PT subpopulations. C, Venn diagram showing the overlap between the differentially expressed genes (DEGs) of PT_VCAM1 cells and failed-repair PT cells. Statistical significance was determined by a hypergeometric test. D, Diffusion map showing the PT cells in snRNA-seq data, coloured by PT subpopulations. This visualisation is based on the first 3 eigenvectors of the diffusion map, highlighting the closest proximity between the PT_VCAM1 and PT_S1_RALYL cells. E, Spatial distribution of cellular composition calculated by Cell2location for PT subpopulations in a representative lupus nephritis (LN) sample. F, Diffusion maps for PT_S1 and PT_VCAM1 cells overlaid with velocity vectors from MultiVelo (top, shown as streamlines) and pseudotime trajectories (bottom). Cells are coloured by PT clusters (top) and inferred pseudotime (bottom), respectively. G, Heatmap of genes differentially expressed along the path 2 trajectory, with cells ordered by pseudotime and genes ordered by their maximum expression values. Representative genes are shown on the right. H, Dot plot displaying normalised regulon specificity scores (RSS) and expression of the top enriched transcription factors (TFs) across PT cell types. I, Three-layer regulatory networks depicting the *cis*-regulatory architecture of TFs, regulatory peaks, and target genes in path 2. Circle sizes represent gene expression ratios, while colour intensities indicate log fold changes (FCs). Only edges with a correlation coefficient greater than 0.05 were retained; edge colour and thickness are for visualisation purposes only and do not convey biological meaning. J, Relative gene expression of *BACH2* in BACH2-overexpressing and control HK-2 cells. Statistical significance was assessed using a 2-sided Student's t-test (****$P < .0001$; n = 5). K, Heatmap displaying z-scaled expression levels of selected DEGs in control and BACH2-overexpressing HK-2 cells. L, Box plot showing PT_VCAM1 signature scores in control and BACH2-overexpressing HK-2 cells. Statistical significance was evaluated using a 2-sided Student's t-test (****$P < .0001$; n = 5). IRI, ischaemia-reperfusion injury.

cell-state transition (Supplementary Fig S11B,C). Both the deviation score of the BACH2 motif and its gene expression were elevated at early stages along the trajectory, suggesting that BACH2 functions as a key transcriptional regulator contributing to the PT_VCAM1-associated injury process (Supplementary Fig S11D,E). To validate the role of BACH2 in promoting injury-related phenotypes, we overexpressed BACH2 in HK-2 cells (Fig 3J and Supplementary Fig S11F) and observed upregulation of injury markers (eg, *VCAM1* and *VIM*), proinflammatory responses (eg, *TNFSF10* and *CX3CL1*), and profibrotic signalling (eg, *ITGA3* and *COL4A1*) (Fig 3K). Consistently, the expression of PT_VCAM1 cell signature genes was significantly increased in BACH2-overexpressing cells (Fig 3L), supporting the functional contribution of BACH2 to the PT_VCAM1 cell phenotype.

PT_VCAM1 cells are involved in the fibrotic niche through ECM remodelling and immune cell recruitment

Intercellular communication is a fundamental process in the repair of injured tissues. To elucidate the impact of ligand-receptor (LR) interactions on the PT_VCAM1 cells and, in turn, the influence of this cell cluster on neighbouring cell types, we integrated single-cell and ST data, incorporating spatial proximity into our analyses (Fig 4A). Specifically, we applied the global Moran's statistic [34], a measure of spatial autocorrelation, to identify spatially coexpressed LR pairs in the CellChat database [35]. We then used COMMOT [36], which incorporates LR competition and interaction distances, to infer niche-specific cell −cell communication networks (Fig 4A). Our analysis found that PT_VCAM1 cells primarily received interactions from

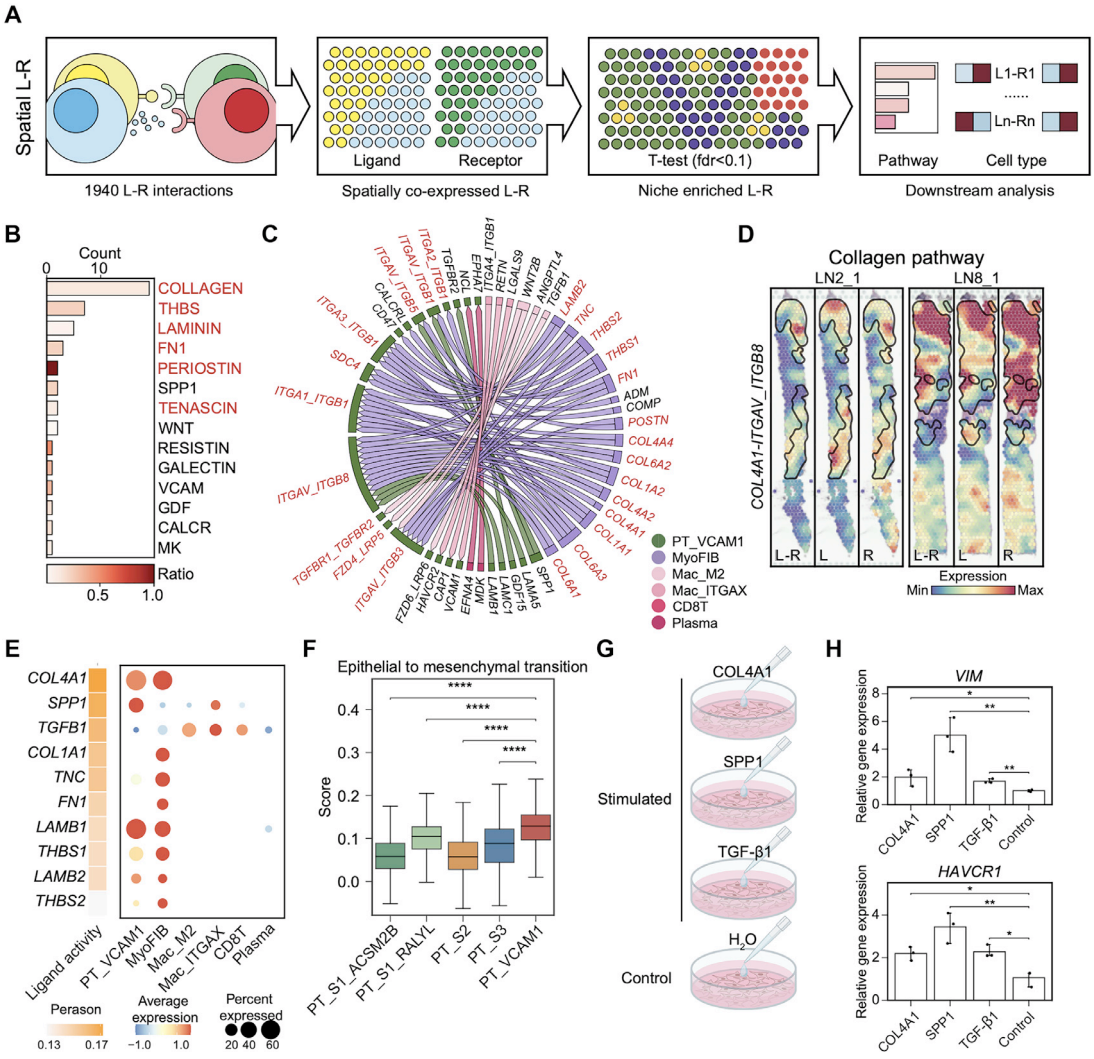

Figure 4. *VCAM1*-expressing proximal tubule (PT_VCAM1)-centric cell−cell interaction network. A, Schematic of the strategy for analysing cell−cell interactions based on spatial transcriptomics (ST) data. B, Bar plots illustrating the enrichment of signalling pathways in interactions between PT_VCAM1, acting as a receiver, and niche 5-specific cell types. C, Chord diagrams depicting interactions between PT_VCAM1, acting as a receiver, and niche 5-specific cell types. D, Smoothed spatial expression of *COL4A1-ITGAV_ITGB8* pairs, *COL4A1,* and *ITGAV_ITGB8* in representative lupus nephritis (LN) samples. Niche 5 is outlined in black. E, Heatmap showing NicheNet's ligand activity predictions with PT_VCAM1-related genes (left) and dot plot depicting the expression patterns of these ligands across niche 5-enriched cell populations (right). F, Box plot depicting the epithelial-mesenchymal transition (EMT) scores across proximal tubule (PT) cell subpopulations. Statistical significance was assessed using a 2-sided Wilcoxon rank-sum test (****$P < .0001$). G, Schematic representation of the strategy for *in vitro* stimulation of human kidney-2 (HK-2) cells, an immortalized human proximal tubular epithelial cell line derived from normal adult kidney. H, Bar plots showing the relative gene expression of *VIM* (top) and *HAVCR1* (bottom) in HK-2 cells across different stimulation conditions. Statistical significance was assessed using a 2-sided Student's t-test (**$P < .01$, *$P < .05$; n = 3 per group). L, ligand; L-R, ligand-receptor; Mac_ITGAX, *ITGAX*-expressing macrophages; Mac_M2, CD163-expressing M2 macrophages; MyoFIB, myofibroblast; R, receptor; TGF, transforming growth factor.

surrounding cells involving ECM components, including collagen, thrombospondin (*THBS*), laminin, fibronectin (*FN1*), periostin (*POSTN*), and tenascin (*TNC*) (Fig 4B,C and Supplementary Table S7). These ECM-encoding genes were predominantly expressed by MyoFIB and PT_VCAM1 cells, which engaged integrin receptors on the PT_VCAM1 cells (Fig 4D and Supplementary Fig S12A-C). Among these ECM components, *TNC*, known to impair tubular integrity and drive kidney fibrosis via integrin signalling, may contribute to the profibrotic niche observed in PT_VCAM1 cells [37].

To examine the impact of these interactions on the gene expression of PT_VCAM1 cells, we applied NicheNet [38] to prioritise ligands modulating upregulated genes in the late stages of path 2 (Fig 4E). Eight out of the top 10 prioritised ligands were epithelial-mesenchymal transition (EMT)-related genes, including *COL4A1, COL1A1, TNC*, and *FN1*, aligning with previous studies that link EMT to kidney fibrosis [39,40] (Supplementary Table S8). *TGFB1* was also identified as a key ligand interacting with *TGFBR1* and *TGFBR2* receptors on the PT_VCAM1 cells (Fig 4E and Supplementary Fig S12D). This ligand is secreted by immune cells, including macrophages and CD8 T cells, and has been demonstrated to induce EMT in kidney disease [41]. The impact of transforming growth factor (TGF)-β1 signalling was supported by our findings, which showed that PT_VCAM1 cells exhibited the highest EMT scores among all PT cell clusters (Fig 4F and Supplementary Fig S12E). To validate whether the predicted ligands promote kidney fibrosis and EMT in PT cells, we stimulated human PT epithelial cells (PTECs) with the top 3 ligands—COL4A1, SPP1, and TGF-β1—and evaluated their effects on *VIM* and *HAVCR1* expression (Fig 4G). Our results demonstrated that all 3 ligands significantly induced higher expression of *VIM* and *HAVCR1* in PTECs (Fig 4H). Furthermore, we also observed a marked upregulation of *BACH2* in PTECs upon *in vitro* stimulation (Supplementary Fig S12F).

We then investigated how PT_VCAM1 cells influence their neighbouring microenvironment and found that PT_VCAM1 cells secreted chemokines such as *CX3CL1* and *CXCL12*, which engaged *CX3CR1* and *CXCR4* on immune cells, facilitating targeted recruitment to injury sites (Supplementary Fig S13A-C and Supplementary Table S7). Concomitantly, local immune cell populations, particularly CD8 T cells, exhibited elevated cytokine secretion and activation signatures in LN samples (Supplementary Fig S13D-G). In parallel, PT_VCAM1 cells produced ECM-related ligands that could bind *CD44* on MyoFIB and CD8 T cells, potentially enhancing cell adhesion and sustaining the fibrotic niche (Supplementary Fig S13B,C). Collectively, these findings reveal the pivotal role of PT_VCAM1 cells in modulating ECM deposition, EMT induction, and immune cell recruitment through spatially coordinated LR interactions, highlighting their central role in pathological tissue remodelling.

GWAS mapping prioritises causal variants facilitating kidney fibrosis in PT_VCAM1 cells

To gain cell-type–specific insights into the role of genetic variants in LN, we performed a fine-mapping genetic analysis using fgwas with an SLE GWAS dataset comprising 208,370 East Asian samples [21] (Fig 5A and Supplementary Fig S14A). As expected, SLE-associated SNPs were significantly enriched in candidate CREs specific to immune cells, such as B cells, Mac_M2, Mac_ITGAX, and CD4 T cells, corroborating their established roles in LN pathogenesis [6,7]. Notably, we also observed significant enrichment of SLE SNPs in CREs specific to endothelial and epithelial cells, particularly PT_VCAM1 cells, suggesting previously unrecognised genetic influences on kidney epithelial cells (Fig 5B). To understand the functional effects of these SNPs, we obtained 26,304 disease-associated SNPs (referred to as "prioritised SNPs") by integrating genome-wide significant SNPs ($P < 5 \times 10^{-8}$) with those that exhibit high posterior probability (posterior probability of association [PPA] > 0.01) across various cell types. Linking these SNPs to gene expression through cell-type–specific accessible peaks revealed 4520 SNP-gene pairs, 34% of which were validated in expression quantitative trait loci (eQTL) studies [42,43] (Supplementary Fig S14B and Supplementary Table S9), demonstrating the high resolution and accuracy of our approach.

To further investigate the expression patterns of genes linked to the prioritised SNPs, we performed gene expression clustering across cell subpopulations, identifying 8 distinct gene clusters (C1-C8; Fig 5C and Supplementary Table S10). Clusters C1 to C4 and C6 were significantly enriched in niche 5 (Supplementary Fig S14C,D), suggesting that the GWAS SNPs have a genetic predisposition for LN progression. For example, SNPs in the *CD44* locus, such as rs2785201, were linked to increased expression of *CD44* in CD4 and CD8 T cells, potentially influencing immune cell recruitment and inflammation via interactions with hyaluronan [44] (Supplementary Fig S15A-C). Moreover, *COL4A1*, which encodes a subunit of type IV collagen, has been identified as a pivotal marker influenced by genetic variants associated with LN susceptibility [45]. We identified a distinct SNP (rs4284503) in a distal CRE specific to the PT_VCAM1 cells, coaccessible with the *COL4A1* promoter (Fig 5D,E). The distal CRE was located within the *COL4A2* gene body and linked to the expression of both *COL4A1* and *COL4A2* (Fig 5F), potentially reflecting the promoter proximity of these 2 genes. Moreover, our results suggest predominant expression of *COL4A1* in PT_VCAM1 cells and MyoFIB, which may drive PT cell injury and promote EMT (Fig 4E,H). The high expression of *COL4A1* in PT_VCAM1 cells was also validated by our SeekSpace data (Supplementary Fig S15D).

Using a gapped k-mer support vector machine (gkm-SVM) approach [46], we identified 63 SNPs that significantly affect the TF binding motif (Supplementary Table S11), including rs4472162, which enhances chromatin accessibility at a *BMP2K* upstream CRE in PT_VCAM1 cells by creating a BACH2 motif (Fig 5G,H). The upregulation of BMP2K promotes the degradation of HNF1B and HNF4A, key TFs essential for PTEC identity [47], aligning with the loss of HNF4A enrichment observed in PT_VCAM1 cells (Fig 3H). Electrophoretic mobility shift assays (EMSAs) further demonstrated that the SLE risk allele (A>T) at rs4472162 significantly enhances BACH2 binding affinity to the *BMP2K* enhancer region (Supplementary Fig S15E,F). Additionally, we also identified a SNP (rs113607426) located within an intron of *SLC17A3*, and the accessibility of this peak was positively associated with the gene expression of 3 solute carrier family 17 member genes (*SLC17A1, SLC17A3, and SLC17A4*) (Supplementary Fig S15G-J). SLC17 transporters are type I phosphate transporters expressed in the kidney and liver [48]. However, the pathogenic roles of these transporters in LN remain unclear. Collectively, these findings reveal how genetic variants converge on specific cell types within LN-enriched niche 5, uncovering the regulatory mechanisms that drive fibrosis and inflammation. These insights provide a framework for understanding genetic predispositions in LN and identifying potential therapeutic targets.

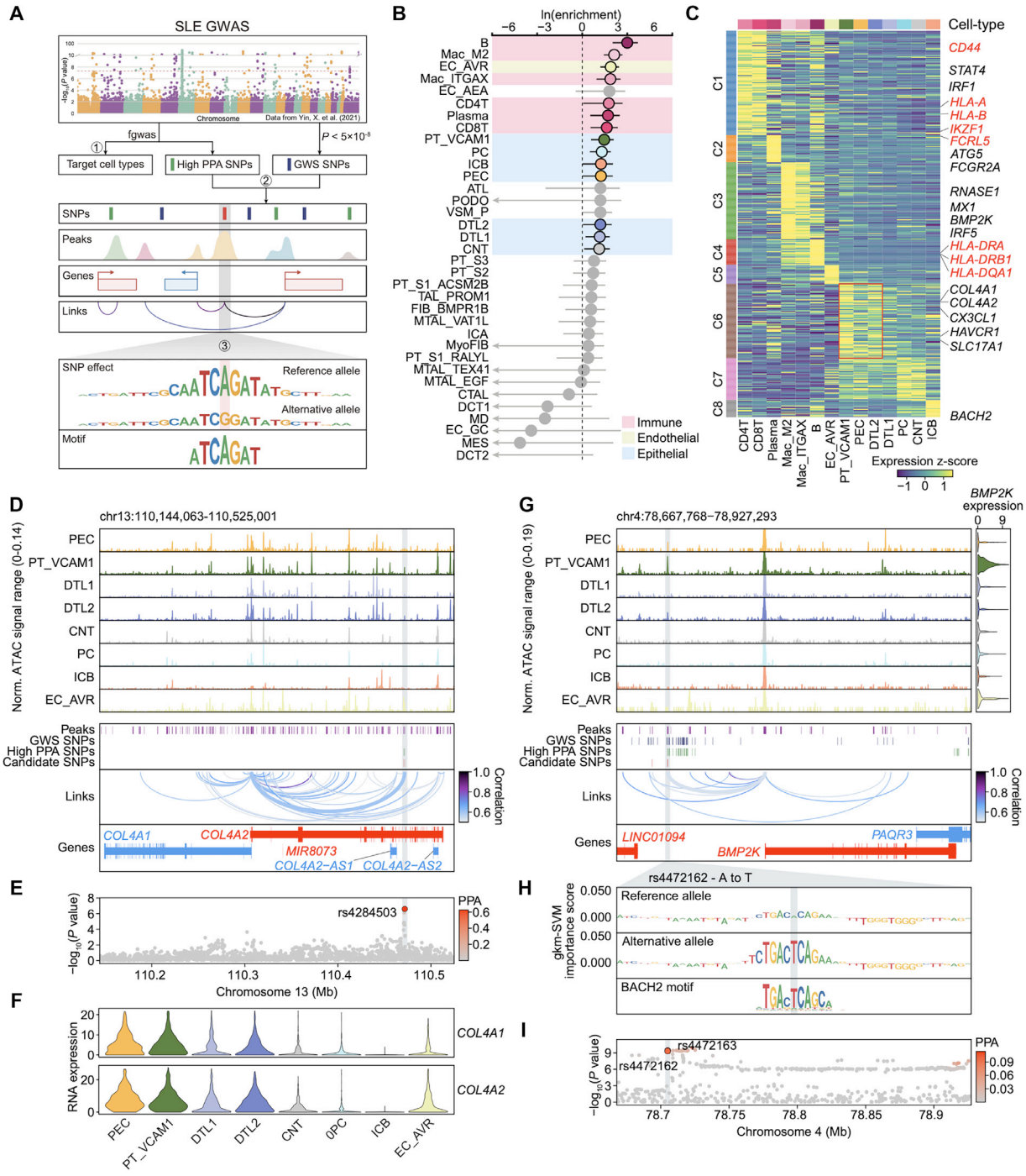

Figure 5. Cell-type-specific genetic risk locus analysis in lupus nephritis (LN). A, Schematic representation of the strategy employed to identify potential causative single-nucleotide polymorphisms (SNPs), their associated gene targets, and the prediction of their impact on transcription factor binding site accessibility. B, Lollipop plot displaying systemic lupus erythematosus (SLE) ln(enrichment) within cell-type–specific *cis*-regulatory elements (CREs). Cell types with positive enrichment and a 95% CI lower bound below zero are shaded in grey. Data represent ln(enrichment) ± 95% CI derived from fgwas. C, Clustered heatmap illustrating the expression profiles of genes associated with candidate SNPs for each cell type. Representative genes are labelled, with gene names in red indicating fine-mapped SNP-to-gene associations supported by public expression quantitative trait loci (eQTL) data from the GTEx portal and the Susztak Lab. D, Normalised chromatin accessibility for cell-type–specific pseudo-bulk tracks surrounding the *COL4A1/COL4A2* locus in SLE heritability-enriched nonimmune cell types. The positions of assay for transposase-accessible chromatin sequencing (ATAC-seq) peaks, genome-wide significant (GWS) SNPs, high posterior probability of association (PPA) SNPs, and candidate functional SNPs are shown below the ATAC-seq tracks. Significant peak-to-gene linkages are indicated by loops connecting the promoter to corresponding peaks. E, Magnified Manhattan plot of the region shown in (D) coloured by PPA level. The candidate SNP is outlined in black. F, Violin plots depicting the expression levels of *COL4A1* and *COL4A2* across the cell types shown in (D). G, As in (D), but for the *BMP2K* locus. *BMP2K* expression levels are shown in the violin plot for each cell type to the right. H, GkmExplain importance scores for the 50 bp region surrounding rs4472162, which creates a BACH2 motif in a CRE linked to *BMP2K* expression. The effect and noneffect alleles for the gapped k-mer support vector machine (gkm-SVM) model are based on the model trained on the VCAM1-expressing proximal tubule (PT_VCAM1) cluster. I, As in (E), but for the region shown in (G). GWAS, genome-wide association studies; PODO, podocyte; PEC, parietal epithelial cell; PT, proximal tubule cell; DTL1, descending thin limb cell type 1; DTL2, descending thin limb cell type 2; ATL, ascending thin limb cell; MTAL_EGF, *EGF*-expressing medullary thick ascending limb cell; MTAL_VAT1L, *VAT1L*-expressing medullary thick ascending limb cell; MTAL_TEX41, *TEX41*-expressing medullary thick ascending limb cell; CTAL, cortical thick ascending limb cell; TAL_PROM1, *PROM1*-expressing thick ascending limb cell; MD, macula densa cell; DCT1, distal convoluted tubule cell type 1; DCT2, distal convoluted

DISCUSSION

Previous studies using single-cell RNA sequencing have provided valuable insights into the roles of immune and epithelial cells in LN [2,4,6,7,49]. However, the detailed cellular organisation and cell–cell interactions within the local microenvironment remain poorly understood. In this study, we employed single-cell multiome sequencing and ST to analyse kidney samples from patients with LN and controls. Our findings revealed a unique LN-associated cellular niche (niche 5), which was positively correlated with serum creatinine and proteinuria levels. This niche, characterised by increased immune cell infiltration and MyoFIB accumulation, also harboured a subpopulation of PT_VCAM1 cells exhibiting a "failed-repair" phenotype. These cells contribute to disease progression by amplifying the inflammatory and profibrotic microenvironment, linking their dysfunction to kidney fibrosis and tubular atrophy—key features predictive of poor kidney outcomes in LN [9,20].

Our study identified niche 5 as a distinct cortical microenvironment of LN, characterised by immune cell infiltration and MyoFIB accumulation—both recognised as contributors to kidney damage [4]. Within this niche, PT_VCAM1 cells emerged as a key epithelial population associated with fibrosis progression, with their abundance significantly higher in cyclophosphamide nonresponders compared with responders. Furthermore, *VCAM1* expression in the tubulointerstitium positively correlated with serum creatinine and proteinuria, highlighting PT_VCAM1 cells and *VCAM1* as potential tissue-level biomarkers of disease severity and treatment response in LN.

Trajectory analysis further demonstrated that PT_VCAM1 cells originate from intermediate-injury PT precursors (PT_S1_RALYL), tracing a continuum from early to late injury states. This finding refines the current understanding of epithelial cell-state transitions in LN and aligns with prior studies on kidney fibrosis [5,20]. Mechanistically, our research underscores the dynamic interplay between PT_VCAM1 cells and local immune cells, which is partially induced by the TGF-β1–mediated EMT process. These insights suggest that TGF-β receptor kinase inhibitors, such as galunisertib, may hold therapeutic potential in mitigating PT fibrotic reprogramming in LN.

Immune cells have long been recognised as contributors to LN pathogenesis [4,7]; our study provides insights into the role of genetic variants within PT_VCAM1 cells associated with kidney fibrosis. Among the identified variants, rs4284503 in the distal region of the *COL4A1* locus was found to enhance collagen deposition via PT_VCAM1 cells. While *COL4A1* overexpression in fibroblasts and endothelial cells has been linked to kidney fibrosis [50], our study highlights a previously unrecognised role of *COL4A1* regulation in PT cells.

Beyond *COL4A1*, we identified additional SLE-associated variants that influence the binding motifs of TFs. Notably, *BMP2K*, encoding bone morphogenetic protein 2-inducible kinase, emerged as a key gene in the pathogenic process. Knockout studies of *BMP2K* have shown that its absence restores normal PTEC function [47], indicating the role of *BMP2K* in disturbing tubular integrity. We identified a distal *BMP2K* variant, rs4472162, that creates a de novo BACH2 binding motif, consistent with our gene regulatory network analysis, positioning BACH2 as a central regulator of the failed-repair PT_VCAM1 program. These findings nominate both BMP2K inhibitors (eg, Cerdulatinib [MedChemExpress] and SGC-AAK1-1) and BACH2 modulators (eg, compound 8) as candidate therapeutic agents for targeting this pathogenic epithelial niche in LN.

Despite the strengths of our integrative approach, several limitations should be acknowledged. The relatively small patient cohort limited our ability to fully capture the heterogeneity of LN. Needle biopsy, required for LN tissue sampling, brings challenges to the comprehensive exploration of kidney injury. Furthermore, the naturally low abundance of immune cells in kidney tissues limited our ability to explore their functional role; sorting immune cells for subsequent investigation could provide deeper insights into the impact of genetic variants on immune cell function. Additionally, 10× multiome workflows require nuclei isolation, which may limit the detection of cytoplasmic transcripts and certain cell states, particularly those of granulocytes. Nevertheless, our work provides a comprehensive understanding of the spatial architecture of LN tissues, the interplay between cell types in pathogenic hotspots, and the regulatory programs associated with kidney injury, laying the groundwork for potential therapeutic strategies targeting both immune and kidney tubular cells.

Competing interests

KQ is the chief scientific advisor of HanGene Biotech and Bassfish Technology. The other authors declare that they have no competing interests.

CRediT authorship contribution statement

Junyu Wang: Writing – original draft, Visualization, Validation, Methodology, Data curation. **Ao Zheng:** Visualization, Methodology, Formal analysis, Data curation. **Nianping Liu:** Writing – original draft, Methodology, Formal analysis, Data curation. **Zhen Tan:** Visualization, Resources. **Yu Shi:** Methodology, Data curation. **Tianyi Ma:** Software, Data curation. **Songwen Luo:** Visualization, Data curation. **Lin Zhu:** Methodology. **Zhou Zhou:** Validation. **Feifei Yuan:** Visualization, Validation. **Tiekun Li:** Visualization. **Yuyan Gong:** Validation, Data curation. **Jingwen Fang:** Visualization. **Lu Liu:** Resources. **Xuejun Zhang:** Resources. **Sang-Cheol Bae:** Resources. **Chikashi Terao:** Resources. **Zhu Chen:** Resources. **Xiaomei Li:** Resources. **Guosheng Wang:** Supervision, Resources. **Kun Qu:** Writing – review & editing, Supervision, Project administration, Funding acquisition, Conceptualization. **Chuang Guo:** Writing – review & editing, Supervision, Resources, Project administration, Funding acquisition, Data curation, Conceptualization.

Acknowledegments

We thank the USTC Supercomputing Center and the School of Life Science Bioinformatics Center for providing computing resources for this project. We also acknowledge the Core Facility

tubule cell type 2; CNT, connecting tubule cell; PC, principal cell; ICA, alpha-intercalated cell; ICB, beta-intercalated cell; EC_AVR, ascending vasa recta endothelial cell; EC_GC, glomerular capillary endothelial cell; EC_AEA, afferent/efferent arteriole endothelial cell; MyoFIB, myofibroblast; FIB_BMPR1B, *BMPR1B*-expressing fibroblast; VSM/P, vascular smooth muscle cell or pericyte; MES, mesangial cell; Mac_M2, *CD163*-expressing M2 macrophage; Mac_ITGAX, *ITGAX*-expressing macrophage.

at the Institute of Health and Medicine, Hefei Comprehensive National Science Center, for providing experimental platforms.

Contributors

CG and KQ conceived the project. GW collected clinical samples and interpreted clinical data with the help of ZC and XL. JW, CG, and KQ designed experiments. JW performed the experiments and conducted the sample preparation with the help of ZT, LZ, ZZ, and TL. JW and AZ performed data analysis with the help of YS, TM, SL, FY, YG, and JF. XZ, S-CB, CT, and LL provided the GWAS data. CG, KQ, JW, NL, and AZ wrote the manuscript with the help of all the other authors. KQ and CG supervised the entire project. All the authors read and approved the final manuscript.

Funding

This work was supported by the National Natural Science Foundation of China grants (32570791 and 32270978 to CG, T2125012 to KQ), the National Key R&D Program of China (2022YFA1303200 to KQ), the Strategic Priority Research Program of Chinese Academy of Sciences (grant number XDB0940301 to KQ), the Fundamental Research Funds for the Central Universities (YD9100002026, YD9100002032, and WK9110000141 to KQ, WK9100000086 to CG), and the Basic Science Research Program through the National Research Foundation of Korea (NRF), funded by the Ministry of Education (NRF-2021R1A6A1A03038899 and NFEC 2023R1A6C101A009 to SCB).

Patient consent for publication

Written informed consent was obtained from all participants.

Ethics approval

Ethical approval was granted by the ethics committee of the First Affiliated Hospital of the University of Science and Technology of China (No. 2024-KY-265).

Provenance and peer review

Not commissioned; externally peer reviewed.

Data availability statement

Processed spatial transcriptomics, snRNA-seq, and snATAC-seq generated in this study are available at the Zenodo data archive (https://doi.org/10.5281/zenodo.15868389). The raw sequencing data generated in this study—including single-cell multiome, spatial transcriptomics, and bulk RNA sequencing (RNA-seq)—have been deposited in the Genome Sequence Archive (GSA) at the BIG Data Center, National Genomics Data Center, China National Center for Bioinformation/Beijing Institute of Genomics, and Chinese Academy of Sciences (accession number: PRJCA035165). The data are publicly accessible at https://ngdc.cncb.ac.cn/gsa-human. The publicly available data sources used in this study are as follows: (1) snRNA-seq and snATAC-seq data from human kidney control samples (Muto et al) were obtained from the Gene Expression Omnibus (GEO) (GSE151302); (2) snRNA-seq data from the human kidney atlas (Lake et al [3]) were obtained from GEO (GSE183277); (3) single-cell RNA sequencing (scRNA-seq) data of human lupus nephritis kidney immune cells (Arazi et al [2]) were accessed from the ImmPort repository (SDY997); (4) Microarray data from human lupus nephritis kidney biopsy samples (Parikh et al [19]) were obtained from GEO (GSE200306); (5) Bulk RNA-seq data (n = 25) from kidney tissues of 16 patients with proliferative LN (Bulusu et al [23]) were obtained from GEO (PRJNA1080019); (6) the GWAS summary statistics of the SLE GWAS dataset, comprising 208,370 East Asian samples, were obtained from the coauthor upon request [11].

Declaration of generative AI and AI-assisted technologies in the writing process

During the preparation of this work the authors used ChatGPT 4.0 in order to improve the language and readability. After using this tool, the authors reviewed and edited the content as needed and take full responsibility for the content of the publication.

Supplementary materials

Supplementary material associated with this article can be found, in the online version, at doi:10.1016/j.ard.2025.08.015.

Orcid

Junyu Wang: http://orcid.org/0009-0000-0621-3435
Ao Zheng: http://orcid.org/0009-0004-6494-4382
Nianping Liu: http://orcid.org/0000-0002-9044-6457
Zhen Tan: http://orcid.org/0000-0002-9988-5587
Tianyi Ma: http://orcid.org/0009-0000-8386-3431
Sang-Cheol Bae: http://orcid.org/0000-0003-4658-1093
Zhu Chen: http://orcid.org/0000-0003-0828-1583
Chuang Guo: http://orcid.org/0000-0002-3912-0793

REFERENCES

[1] Mok CC, Teng YKO, Saxena R, Tanaka Y. Treatment of lupus nephritis: consensus, evidence and perspectives. Nat Rev Rheumatol 2023;19(4):227–38. doi: 10.1038/s41584-023-00925-5.
[2] Arazi A, Rao DA, Berthier CC, Davidson A, Liu Y, Hoover PJ, et al. The immune cell landscape in kidneys of patients with lupus nephritis. Nat Immunol 2019;20(7):902–14. doi: 10.1038/s41590-019-0398-x.
[3] Lake BB, Menon R, Winfree S, Hu Q, Melo Ferreira R, Kalhor K, et al. An atlas of healthy and injured cell states and niches in the human kidney. Nature 2023;619(7970):585–94. doi: 10.1038/s41586-023-05769-3.
[4] Chen W, Jin B, Cheng C, Peng H, Zhang X, Tan W, et al. Single-cell profiling reveals kidney CD163(+) dendritic cell participation in human lupus nephritis. Ann Rheum Dis 2024;83(5):608–23. doi: 10.1136/ard-2023-224788.
[5] Li H, Dixon EE, Wu H, Humphreys BD. Comprehensive single-cell transcriptional profiling defines shared and unique epithelial injury responses during kidney fibrosis. Cell Metab 2022;34(12) 1977-98.e9. doi: 10.1016/j.cmet.2022.09.026.
[6] Tang Y, Zhang Y, Li X, Xu R, Ji Y, Liu J, et al. Immune landscape and the key role of APOE+ monocytes of lupus nephritis under the single-cell and spatial transcriptional vista. Clin Transl Med 2023;13(4):e1237. doi: 10.1002/ctm2.1237.
[7] Wu C, Jiang S, Chen Z, Li T, Gu X, Dai M, et al. Single-cell transcriptomics reveal potent extrafollicular B cell response linked with granzyme K(+) CD8 T cell activation in lupus kidney. Ann Rheum Dis 2024;84(3):451–66. doi: 10.1136/ard-2024-225876.
[8] Muto Y, Wilson PC, Ledru N, Wu H, Dimke H, Waikar SS, et al. Single cell transcriptional and chromatin accessibility profiling redefine cellular heterogeneity in the adult human kidney. Nat Commun 2021;12(1):2190. doi: 10.1038/s41467-021-22368-w.
[9] Muto Y, Dixon EE, Yoshimura Y, Wu H, Omachi K, Ledru N, et al. Defining cellular complexity in human autosomal dominant polycystic kidney disease by multimodal single cell analysis. Nat Commun 2022;13(1):6497. doi: 10.1038/s41467-022-34255-z.
[10] Abedini A, Levinsohn J, Klötzer KA, Dumoulin B, Ma Z, Frederick J, et al. Single-cell multi-omic and spatial profiling of human kidneys implicates the

fibrotic microenvironment in kidney disease progression. Nat Genet 2024;56 (8):1712–24. doi: 10.1038/s41588-024-01802-x.
[11] Yin X, Kim K, Suetsugu H, Bang SY, Wen L, Koido M, et al. Meta-analysis of 208370 East Asians identifies 113 susceptibility loci for systemic lupus erythematosus. Ann Rheum Dis 2021;80(5):632–40. doi: 10.1136/annrheumdis-2020-219209.
[12] Gallagher MD, AS Chen-Plotkin. The post-GWAS era: from association to function. Am J Hum Genet 2018;102(5):717–30. doi: 10.1016/j.ajhg.2018.04.002.
[13] Hon CC, Ramilowski JA, Harshbarger J, Bertin N, Rackham OJ, Gough J, et al. An atlas of human long non-coding RNAs with accurate 5′ ends. Nature 2017;543(7644):199–204. doi: 10.1038/nature21374.
[14] Hao Y, Stuart T, Kowalski MH, Choudhary S, Hoffman P, Hartman A, et al. Dictionary learning for integrative, multimodal and scalable single-cell analysis. Nat Biotechnol 2024;42(2):293–304. doi: 10.1038/s41587-023-01767-y.
[15] Davidson A. What is damaging the kidney in lupus nephritis? Nat Rev Rheumatol 2016;12(3):143–53. doi: 10.1038/nrrheum.2015.159.
[16] Melo Ferreira R, Sabo AR, Winfree S, Collins KS, Janosevic D, Gulbronson CJ, et al. Integration of spatial and single-cell transcriptomics localizes epithelial cell-immune cross-talk in kidney injury. JCI Insight 2021;6(12):e147703. doi: 10.1172/jci.insight.147703.
[17] Kleshchevnikov V, Shmatko A, Dann E, Aivazidis A, King HW, Li T, et al. Cell2location maps fine-grained cell types in spatial transcriptomics. Nat Biotechnol 2022;40(5):661–71. doi: 10.1038/s41587-021-01139-4.
[18] Xu H, Wang S, Fang M, Luo S, Chen C, Wan S, et al. SPACEL: deep learning-based characterization of spatial transcriptome architectures. Nat Commun 2023;14(1):7603. doi: 10.1038/s41467-023-43220-3.
[19] Parikh SV, Malvar A, Song H, Shapiro J, Mejia-Vilet JM, Ayoub I, et al. Molecular profiling of kidney compartments from serial biopsies differentiate treatment responders from non-responders in lupus nephritis. Kidney Int 2022;102(4):845–65. doi: 10.1016/j.kint.2022.05.033.
[20] Kirita Y, Wu H, Uchimura K, Wilson PC, Humphreys BD. Cell profiling of mouse acute kidney injury reveals conserved cellular responses to injury. Proc Natl Acad Sci U S A 2020;117(27):15874–83. doi: 10.1073/pnas.2005477117.
[21] Hinze C, Kocks C, Leiz J, Karaiskos N, Boltengagen A, Cao S, et al. Single-cell transcriptomics reveals common epithelial response patterns in human acute kidney injury. Genome Med. Genome Med. 2022;14(1):103. doi: 10.1186/s13073-022-01108-9.
[22] Klocke J, Kim SJ, Skopnik CM, Hinze C, Boltengagen A, Metzke D, et al. Urinary single-cell sequencing captures kidney injury and repair processes in human acute kidney injury. Kidney Int 2022;102(6):1359–70. doi: 10.1016/j.kint.2022.07.032.
[23] Bulusu SN, Bavikatte AN, Shah S, Murthy SSN, Kommoju V, Mariaselvam CM, et al. Renal and peripheral blood transcriptome signatures that predict treatment response in proliferative lupus nephritis-a prospective study. Immunology 2025;174(4):470–80. doi: 10.1111/imm.13891.
[24] Haghverdi L, Buettner F, Theis FJ. Diffusion maps for high-dimensional single-cell analysis of differentiation data. Bioinformatics 2015;31(18):2989–98. doi: 10.1093/bioinformatics/btv325.
[25] Wolf FA, Hamey FK, Plass M, Solana J, Dahlin JS, Göttgens B, et al. PAGA: graph abstraction reconciles clustering with trajectory inference through a topology preserving map of single cells. Genome Biol 2019;20(1):59. doi: 10.1186/s13059-019-1663-x.
[26] Li C, Virgilio MC, Collins KL, Welch JD. Multi-omic single-cell velocity models epigenome-transcriptome interactions and improves cell fate prediction. Nat Biotechnol 2023;41(3):387–98. doi: 10.1038/s41587-022-01476-y.
[27] Setty M, Kiseliovas V, Levine J, Gayoso A, Mazutis L, Pe'er D. Characterization of cell fate probabilities in single-cell data with Palantir. Nat Biotechnol 2019;37(4):451–60. doi: 10.1038/s41587-019-0068-4.
[28] Bravo González-Blas C, De Winter S, Hulselmans G, Hecker N, Matetovici I, Christiaens V, et al. SCENIC+: single-cell multiomic inference of enhancers and gene regulatory networks. Nat Methods 2023;20(9):1355–67. doi: 10.1038/s41592-023-01938-4.
[29] Ledru N, Wilson PC, Muto Y, Yoshimura Y, Wu H, Li D, et al. Predicting proximal tubule failed repair drivers through regularized regression analysis of single cell multiomic sequencing. Nat Commun 2024;15(1):1291. doi: 10.1038/s41467-024-45706-0.
[30] Hao S, Bellner L, Zhao H, Ratliff BB, Darzynkiewicz Z, Vio CP, et al. NFAT5 is protective against ischemic acute kidney injury. Hypertension 2014;63(3): e46–52. doi: 10.1161/HYPERTENSIONAHA.113.02476.
[31] Yoo EJ, Oh KH, Piao H, Kang HJ, Jeong GW, Park H, et al. Macrophage transcription factor TonEBP promotes systemic lupus erythematosus and kidney injury via damage-induced signaling pathways. Kidney Int 2023;104(1):163–80. doi: 10.1016/j.kint.2023.03.030.
[32] Piret SE, Guo Y, Attallah AA, Horne SJ, Zollman A, Owusu D, et al. Kruppel-like factor 6-mediated loss of BCAA catabolism contributes to kidney injury in mice and humans. Proc Natl Acad Sci U S A 2021;118(23):e2024414118. doi: 10.1073/pnas.2024414118.
[33] Zhou Y, Wu H, Zhao M, Chang C, Lu Q. The Bach family of transcription factors: a comprehensive review. Clin Rev Allergy Immunol 2016;50(3):345–56. doi: 10.1007/s12016-016-8538-7.
[34] Li Z, Wang T, Liu P, Huang Y. SpatialDM for rapid identification of spatially co-expressed ligand-receptor and revealing cell-cell communication patterns. Nat Commun 2023;14(1):3995. doi: 10.1038/s41467-023-39608-w.
[35] Jin S, Guerrero-Juarez CF, Zhang L, Chang I, Ramos R, Kuan CH, et al. Inference and analysis of cell-cell communication using CellChat. Nat Commun 2021;12(1):1088. doi: 10.1038/s41467-021-21246-9.
[36] Cang Z, Zhao Y, Almet AA, Stabell A, Ramos R, Plikus MV, et al. Screening cell-cell communication in spatial transcriptomics via collective optimal transport. Nat Methods 2023;20(2):218–28. doi: 10.1038/s41592-022-01728-4.
[37] Zhu H, Liao J, Zhou X, Hong X, Song D, Hou FF, et al. Tenascin-C promotes acute kidney injury to chronic kidney disease progression by impairing tubular integrity via alphavbeta6 integrin signaling. Kidney Int 2020;97(5):1017–31. doi: 10.1016/j.kint.2020.01.026.
[38] Browaeys R, Saelens W, Saeys Y. NicheNet: modeling intercellular communication by linking ligands to target genes. Nat Methods 2020;17(2):159–62. doi: 10.1038/s41592-019-0667-5.
[39] Grande MT, Sánchez-Laorden B, López-Blau C, De Frutos CA, Boutet A, Arévalo M, et al. Snail1-induced partial epithelial-to-mesenchymal transition drives renal fibrosis in mice and can be targeted to reverse established disease. Nat Med 2015;21(9):989–97. doi: 10.1038/nm.3901.
[40] Lovisa S, LeBleu VS, Tampe B, Sugimoto H, Vadnagara K, Carstens JL, et al. Epithelial-to-mesenchymal transition induces cell cycle arrest and parenchymal damage in renal fibrosis. Nat Med 2015;21(9):998–1009. doi: 10.1038/nm.3902.
[41] Shen B, Liu X, Fan Y, Qiu J. Macrophages regulate renal fibrosis through modulating TGFbeta superfamily signaling. Inflammation 2014;37(6):2076–84. doi: 10.1007/s10753-014-9941-y.
[42] Liu H, Doke T, Guo D, Sheng X, Ma Z, Park J, et al. Epigenomic and transcriptomic analyses define core cell types, genes and targetable mechanisms for kidney disease. Nat Genet 2022;54(7):950–62. doi: 10.1038/s41588-022-01097-w.
[43] Consortium GTEx. The GTEx Consortium atlas of genetic regulatory effects across human tissues. Science 2020;369(6509):1318–30. doi: 10.1126/science.aaz1776.
[44] Kadoya H, Yu N, Schiessl IM, Riquier-Brison A, Gyarmati G, Desposito D, et al. Essential role and therapeutic targeting of the glomerular endothelial glycocalyx in lupus nephritis. JCI Insight 2020;5(19):e131252. doi: 10.1172/jci.insight.131252.
[45] Chung SA, Brown EE, Williams AH, Ramos PS, Berthier CC, Bhangale T, et al. Lupus nephritis susceptibility loci in women with systemic lupus erythematosus. J Am Soc Nephrol 2014;25(12):2859–70. doi: 10.1681/ASN.2013050446.
[46] Turner AW, Hu SS, Mosquera JV, Ma WF, Hodonsky CJ, Wong D, et al. Single-nucleus chromatin accessibility profiling highlights regulatory mechanisms of coronary artery disease risk. Nat Genet 2022;54(6):804–16. doi: 10.1038/s41588-022-01069-0.
[47] Mao L, Zhang T, Li Z, Yao W, Cai Y, Li C, et al. Kidney repair through chemically-induced revitalization of renal tubular epithelial cell. Cell Press; 2024 in press. doi: 10.17632/bz47sbmtw2.1.
[48] Reimer RJ. SLC17: a functionally diverse family of organic anion transporters. Mol Aspects Med 2013;34(2-3):350–9. doi: 10.1016/j.mam.2012.05.004.
[49] Der E, Suryawanshi H, Morozov P, Kustagi M, Goilav B, Ranabothu S, et al. Tubular cell and keratinocyte single-cell transcriptomics applied to lupus nephritis reveal type I IFN and fibrosis relevant pathways. Nat Immunol 2019;20(7):915–27. doi: 10.1038/s41590-019-0386-1.
[50] Li H, Li D, Ledru N, Xuanyuan Q, Wu H, Asthana A, et al. Transcriptomic, epigenomic, and spatial metabolomic cell profiling redefines regional human kidney anatomy. Cell Metab 2024;36(5):1105–25. e10. doi: 10.1016/j.cmet.2024.02.015.